Microwave phase detection of coherent population trapping resonance in Cs vapor cell

MICHAEL PETERSEN[1,*], MOUSTAFA ABDEL HAFIZ[1], EMERIC DE CLERCQ[2], AND RODOLPHE BOUDOT[1]

[1] FEMTO-ST, CNRS, UBFC, ENSMM, 26 chemin de l'Epitaphe 25030 Besançon Cedex, France
[2] SYRTE, Observatoire de Paris, CNRS, Sorbonne Université, Paris, France
[*] Corresponding author: rodolphe.boudot@femto-st.fr

Compiled February 2, 2022

We report a phase-sensitive microwave detection setup for spectroscopy of coherent population trapping (CPT) resonance in a Cs vapor cell. In this scheme, the optically-carried microwave interrogation signal that interacts with atoms is detected by a fast photodiode at the cell output and is then mixed with the local oscillator microwave signal itself. This detection scheme produces at the output of the microwave mixer a dispersive CPT signal that can be directly used for correction of the local oscillator frequency onto the atomic resonance. The evolution of the dispersive CPT resonance signal with the laser power is briefly reported. With this detection scheme, we demonstrate the operation of a CPT atomic clock with a short-term fractional frequency stability of 1×10^{-11} at 1 s, in good agreement with the slope of the frequency discriminator and the residual microwave phase noise of the setup.

OCIS codes: (020.0020) Atomic and molecular physics; (020.1670) Coherent optical effects;(120.3930) Metrological instrumentation; (300.6320) Spectroscopy, high-resolution.

http://dx.doi.org/10.1364/ao.XX.XXXXXX

1. INTRODUCTION

Coherent population trapping (CPT) spectroscopy [1–4] consists of making atoms interact with a dual-frequency optical field such that two atomic ground-states are connected to a common excited state. Using this Λ-type interaction scheme, atoms are trapped in a specific quantum dark state in which the initially-opaque atomic medium becomes transparent for the incident light. This quantum interference process permits then the detection of narrow atomic resonances that can be exploited in a relevant number of applications including high-resolution laser spectroscopy [5], atomic clocks [6–13], sensors [14, 15], slow-light experiments [16], or laser cooling [17].

In CPT spectroscopy, the CPT resonance is usually detected as an increase of the light power transmitted through the vapor cell due to increased transparency of the atomic vapor. This detection scheme is simple and efficient since it basically requires the use of a slow photodiode as an optical power detector at the cell output. However, this standard detection scheme also suffers from drawbacks. First, the CPT resonance is usually detected in the bottom of a homogeneously-broadened absorption profile over a dc background level. The latter is induced by residual background light that crosses the cell, without contributing to CPT interaction, and limits the contrast and signal-to-noise ratio of the CPT resonance. Second, the signal to noise ratio of the CPT resonance is degraded by several noise processes, including mainly the photon shot noise, the laser amplitude (AM) noise and the laser frequency (FM) noise through the FM-AM conversion process. These noise sources are known to be important contributions to the short-term frequency stability of CPT vapor cell clocks [9, 10]. Third, the CPT resonance can not be directly used for stabilization of the probing microwave field onto the atomic resonance. Thus, a dispersive zero-crossing error signal is generally extracted from the original resonance signal with a lock-in amplifier-based synchronous modulation stage. This subsequent frequency modulation of the local oscillator (LO) induces an aliasing effect named Dick effect [18–20] or intermodulation effect [21] that can limit the clock short-term frequency stability.

Alternative approaches have been proposed for the detection of CPT resonances. A straightforward method consists of detecting the reduction of fluorescence photons emitted by atoms in the dark state [1, 22]. In other studies, placing the atomic cell in an electromagnetic cavity can produce an oscillating magnetization responsible for a coherent signal emission observed at the atomic ground state hyperfine transition frequency [8]. Also, the direct detection of microwaves generated through stimulated Raman scattering (SRS) [23], electromagnetically-induced transparency (EIT) or CPT towards the construction of cell-based optoelectronic oscillators [23–27], has been reported.

In this paper, we investigate an alternative method for detection of CPT resonance in a Cs vapor cell using a microwave phase

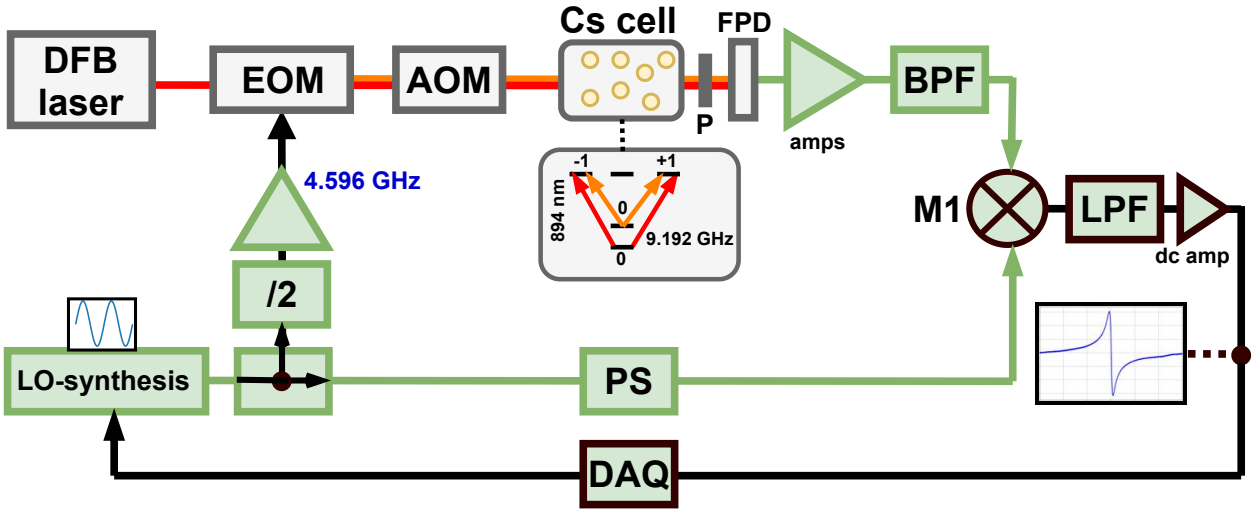

Fig. 1. (Color online) Simplified schematic of the CPT-based Cs cell clock experiment, with microwave phase detection of the CPT resonance. A dual-frequency optical field is generated by the combination of a distributed-feedback (DFB) laser and an external fibered Mach-Zehnder electro-optic modulator (EOM). An acousto-optic modulator (AOM) is used to shift the laser frequency and control the laser power. A Michelson delay-line system, not shown here, is used to produce the push-pull optical pumping (PPOP) scheme. The light is then sent into a buffer-gas filled Cs vapor cell. At the cell output, the microwave-modulated light that crossed the atomic vapor is detected by a fast photodiode (FPD). The optically-carried 9.192 GHz signal is then band-pass filtered, amplified and sent to the RF port of a microwave mixer. This mixer, fed at its LO port by the synthesizer direct output at 9.192 GHz, delivers a dispersive error signal that can be used for direct stabilization of the synthesizer output frequency. P: polarizer, PS: microwave phase shifter, LPF: low-pass filter, BPF: band-pass filter, DAQ: data acquisition card. The inset (below the cell) shows the CPT diagram involved in the PPOP technique. The second inset shows the dispersive CPT signal at the mixer output.

detection scheme. In this method, the standard photodiode at the output of the vapor cell is replaced by a fast photodiode from which the optically-carried microwave signal that probed the atomic vapor and experienced the atomic resonator-induced phase shift is extracted. This signal is then mixed with the original microwave interrogation field in order to produce a dispersive CPT signal, centered at null Raman detuning. A simple theoretical model, in correct agreement with experimental data, was developed to qualitatively predict the microwave phase variation at the cell output. The experimental dependence of the dispersive error signal shape on laser power is briefly studied. To illustrate a possible application of this detection scheme, the dispersive signal at the mixer output was used for direct stabilization of the local oscillator frequency to the Cs clock transition frequency. The clock short-term frequency stability is measured at the level of 1×10^{-11} at 1 s, in good agreement with the slope of the frequency discriminator and the residual phase noise of the setup at 9.192 GHz.

2. EXPERIMENTAL SET-UP

Figure 1 presents the typical experimental setup. The optical part of the setup is inspired by the one described in [11]. The laser source is a 1-MHz linewidth Distributed Feedback (DFB) diode laser tuned on the Cs D_1 line at 894.6 nm. A 70 dB optical isolation stage (not shown on Fig. 1) is used at the output of the laser to prevent optical feedback. The optical field is modulated with a fibered Mach-Zehnder electro-optic modulator (MZ EOM). The EOM is driven by a 4.596 GHz signal, extracted from a 9.192 GHz microwave synthesizer using a by-2 frequency divider and a microwave amplifier, with a power of about 22 dBm. This modulation creates two first-order optical sidebands frequency-split by 9.192 GHz, ultimately used for producing the CPT interaction. The optical carrier at the EOM output is kept strongly rejected by fine tuning of the EOM dc bias. At the output of the EOM, a fraction of the light is used (not shown on Fig. 1 for clarity) for laser frequency stabilization using dual-frequency sub-Doppler spectroscopy [28, 29]. At the output of the EOM, the light is sent into an acousto-optical modulator (AOM) driven with a radiofrequency signal at 122 MHz. This AOM is used to compensate for the optical frequency shift induced by the presence of buffer gas in the CPT cell and can also be used for laser power control. A Michelson delay-line and polarization orthogonalizer system (not shown on Fig. 1) is used to produce the so-called push-pull optical pumping (PPOP) scheme [30] that helps to increase the number of atoms that participate to the 0-0 clock transition. The optically-carried microwave signal is then sent in a 2-cm diameter and 5-cm long buffer-gas filled Cs vapor cell (15 Torr of N_2-Ar buffer gas mixture, with $P_{Ar}/P_{N_2} = 0.6$) with a beam diameter of about 1 cm. The cell is maintained into a temperature-stabilized physics package. A solenoid is available for application of a static magnetic field ($B \approx 10\ \mu$T) parallel to the laser beam propagation. This ensemble is surrounded by a double-layer mu-metal magnetic shield. At the output of the cell, a convergent lens is used to focus the laser beam onto a fast photodiode. A quarter wave plate and a linear polarizer is inserted right after the cell to remove light from one of the PPOP interferometer, as to avoid interference between the two arms and then make possible the detection of the microwave beatnote. The microwave beatnote signal at 9.192 GHz extracted from the fast photodiode is amplified by an ensemble of three serial amplifiers with a total gain of about 70 dB, filtered with a microwave band-pass filter (bandwidth < 50 MHz) and finally sent to the RF port of a microwave mixer. The LO port of the mixer is driven by the 9.192 GHz signal coming directly from the

synthesizer output. A microwave phase shifter is also placed in the LO arm of the bench to adjust the phase difference between the two inputs of the mixer. The microwave mixer delivers then a dispersive clock error signal that can be used for direct stabilization of the synthesizer output frequency on the clock transition frequency.

3. THEORETICAL INSIGHT

In the setup described in Fig. 1, that can be seen as an analog of the Mach-Zehnder interferometer in the microwave domain, a microwave signal, split into two arms, is, in one of them, optically-carried, phase-shifted in the atomic cell resonator through the CPT phenomenon, extracted back using a fast photodiode, before being mixed with the initial microwave signal. The mixer, used as phase detector, delivers then a voltage signal that is proportional to the phase difference between the two mixer inputs. In a simplified model where any phase variation induced by optical or microwave components of the setup are neglected, the phase difference measured at the mixer output corresponds then to the phase variation experienced by the optically-carried microwave signal along the cell. The purpose of this section is then to qualitatively predict this cell-induced phase variation using a simplified theoretical model. We consider the atomic vapor as an homogeneous, isotropic, and linear medium. In this case, the phase delay of an electromagnetic wave after passing through a cell of length L is given by $\varphi = n(\omega/c)L$, with n the refractive index, ω the angular frequency of the wave and c the speed of light in vacuum. n is linked to the real part of the electric susceptibility χ' by $n = \sqrt{1+\chi'} \approx 1 + \chi'/2$. In our experimental conditions, $|\chi'|$ is estimated to be less than 10^{-6}, which justifies this approximation.

In the following, we show how the susceptibility can be calculated from the atomic properties of the system, before giving an estimation of the phase difference measured in next sections. For this analysis, we consider two hyperfine energy levels, the so-called clock levels, labeled 1 and 2, of the Cs ground state, and an excited level noted 3. We assume the presence of two laser fields, of angular frequencies ω_1, ω_2 (optical CPT sidebands described in section 2), quasi-resonant with the optical transitions $(1-3)$ and $(2-3)$, respectively. The susceptibility related to each transition $(i-3)$, $i = 1, 2$, is given by:

$$\chi'_i = \frac{n_{Cs}\, d_{i3}^2}{\epsilon_0 \hbar\, \Omega_{i3}} 2\mathrm{Re}(\rho_{i3}), \tag{1}$$

where n_{Cs} is the Cs atomic density in the vapor, d_{i3} the electric dipole moment of the optical transition $(i-3)$, $\hbar$ the reduced Planck constant, ϵ_0 the vacuum permittivity, Ω_{i3} the Rabi frequency driving the $i-3$ transition and $\mathrm{Re}(\rho_{i3})$ the real part of the optical coherence ρ_{i3} in the density matrix formalism. For the Cs D_1 line considered here, we note $d_{13} = d_{23} = d$. Moreover, we assume in the following equal Rabi frequencies, such that $\Omega_{13} = \Omega_{23} = \Omega$.

The expression of the optical coherences in the steady state were established by Vanier *et al.* [31] using a perturbation approach:

$$\begin{cases} \mathrm{Re}(\rho_{13}) = \dfrac{\Omega/4}{\Gamma^2/4 + \delta_1^2}\left(\delta_1 - \Gamma\,\mathrm{Im}(\rho_{12})\right), \\ \mathrm{Re}(\rho_{23}) = \dfrac{\Omega/4}{\Gamma^2/4 + \delta_2^2}\left(\delta_2 + \Gamma\,\mathrm{Im}(\rho_{12})\right), \\ \mathrm{Re}(\rho_{13}) - \mathrm{Re}(\rho_{23}) = \dfrac{\Omega}{\Gamma^2 + \delta_R^2}\left(\delta_R - 2\Gamma\,\mathrm{Im}(\rho_{12})\right), \end{cases} \tag{2}$$

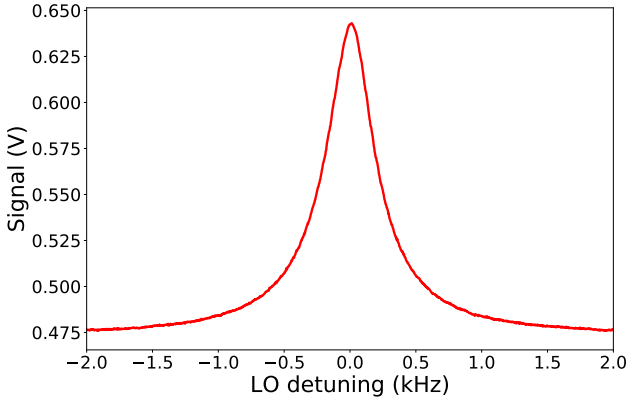

Fig. 2. (Color online) CPT resonance obtained with the standard CPT detection scheme.

where Γ is the full relaxation rate of the excited level (spontaneous emission and effect of collisions with the buffer gas molecules). We consider equal relaxation rates towards 1-and-2 levels. δ_1, δ_2 are the optical detuning of the first lateral bandwidth with respect to the transitions $(1-3)$ and $(2-3)$, respectively. We consider that both lateral bands are scanned around the optical resonances, so that $\delta_2 = -\delta_1$, $\delta_1 - \delta_2 = \delta_R$, $\delta_1^2 = \delta_2^2 = \delta_R^2/4$, with δ_R the Raman detuning. $\mathrm{Im}(\rho_{12})$ stands for the imaginary part of the ground state coherence ρ_{12} and is given by [31]:

$$\mathrm{Im}(\rho_{12}) = \frac{\Omega^2}{2\Gamma} \frac{\delta_R}{(\Delta/2)^2 + \delta_R^2}, \tag{3}$$

with $\Delta/2 = \gamma_c^2 + \Omega^2/\Gamma$ being the half-width of the CPT resonance, and γ_c the relaxation rate of the hyperfine coherence.

Several approximations are used in order to simplify the expression of the resulting phase difference at the output of the mixer. The Doppler effect is not taken into account. We also neglect in the computation of both χ'_i the contribution of the other optical transition, 9 GHz apart, and then far from the main resonance. We also assume that the optical angular frequency difference is small, so that we can use $\omega_1 \approx \omega_2 = \omega$ in the computation of the final phase difference. For the sake of simplicity, we also neglected the attenuation of laser intensities along the cell length, so that the susceptibilities can be considered constant along the cell length. With this, the phase shift between both laser fields at the cell output is calculated by $\Delta\varphi \approx (n(\omega_1) - n(\omega_2))(\omega/c)L \approx (\chi'_1 - \chi'_2)(\omega/c)L/2$. Using Eqs. (1, 2, 3), we finally obtain:

$$\Delta\varphi = L\frac{n_{Cs}\, d^2 \omega}{\hbar\, \epsilon_0\, c}\left[1 - \frac{\Omega^2}{(\Delta/2)^2 + \delta_R^2}\right]\frac{\delta_R}{\Gamma^2 + \delta_R^2}. \tag{4}$$

Close to resonance, the bracketed term is reduced to the fraction, which exhibits a narrow resonance of width Δ around $\delta_R = 0$. As $\delta_R^2 << \Gamma^2$ in the denominator of the last term, a dispersive curve of same width than the transmission curve is expected.

4. EXPERIMENTAL RESULTS

A. First signals

We started our experiments by performing standard CPT spectroscopy. In this case, a standard photodiode replaces the fast

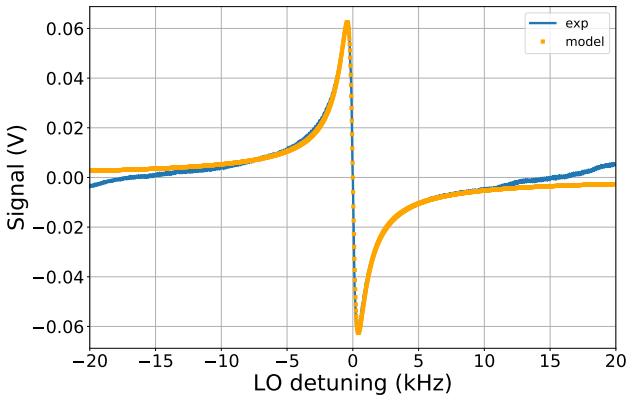

Fig. 3. (Color online) Dispersive CPT resonance signal obtained with the microwave phase detection scheme. The cell temperature is 35.1°C. The laser power P_i is 780 μW. The static magnetic field is 10 μT. Here an offset of -0.125 V was added to the curve such that the zero-crossing is centered. Considering a mixer sensitivity of about 0.215 V/rad, the phase variation at resonance is about 0.57 rad.

.

photodiode shown in Fig. 1. The CPT resonance (0-0 clock transition) observed in transmission is shown on Fig. 2. The cell temperature is 38°C while the total laser power P_i at the cell input is 500 μW. The contrast of the CPT resonance C, defined as the ratio between the CPT signal amplitude and the dc background level, is about 34.7 %. The CPT resonance linewidth is 480 Hz.

We implemented then the setup shown in Fig. 1. Figure 3 shows a dispersive CPT resonance signal detected at the output of the low-pass filter that follows the microwave mixer. This signal is obtained for a cell temperature of 35.1°C and a laser power P_i at the cell input of 780 μW. At low Raman detuning, this signal exhibits a signal amplitude S of 0.124 V (that corresponds to a phase variation of about 0.57 rad) for a linewidth $\Delta\nu$ of 756 Hz, yielding a slope of 1.64×10^{-4} V/Hz. For comparison, Figure 3 shows the phase difference computed with Eq. (4) in the given experimental conditions. The used parameter values are $d = 1.23 \times 10^{-29}$ C.m [32], $\omega = 2.106 \times 10^{15}$ rad/s, $\Omega = 2 \times 10^6$ rad/s adjusted on the resonance width, $n_{Cs} = 0.125 \times 1.2 \times 10^{17}$ atoms/m^3 [33] (we estimate to 12.5% the fraction of atoms involved in each optical transition), $\Gamma = 1.63 \times 10^9$ rad/s [34], $\gamma_c = 203$ rad/s [35], $L = 5 \times 10^{-2}$ m. The model yields a peak-to-peak amplitude of 0.48 rad, to be compared with about 0.57 rad for experimental data. Model amplitude was then adjusted to the experimental value in Volt in order to compare line shapes in Fig. 3. The line shapes are close, except at high detuning.

B. Spectroscopy of the clock signal with laser power

Figure 4 shows the dispersive signal for several values of the laser power entering the cell. For all spectra, we tuned the microwave phase shifter before data recording such that the signal symmetry was optimal. When reducing the laser power, we observe that the best symmetry is obtained for values approaching a null dc background offset. Figure 5 resumes the signal amplitude S, linewidth (FWHM) and S/FWHM ratio of the dispersive signal as a function of the laser power. These three parameters tend to increase with the laser power, yielding a maximized

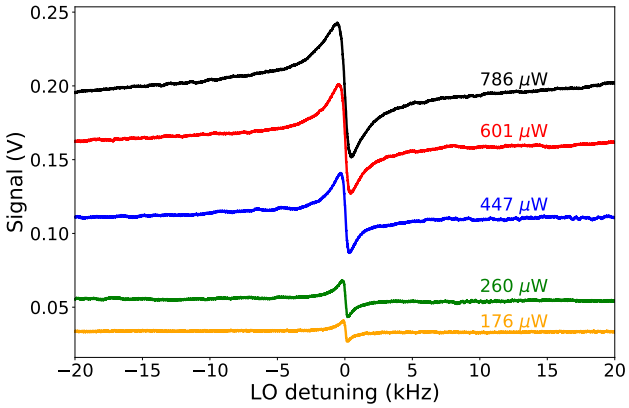

Fig. 4. (Color online) Dispersive CPT signal at the output of the mixer for several values of the total laser power that enters into the cell. The phase shifter is adjusted before each spectrum recording to get a symmetric signal. The cell temperature is 28°C.

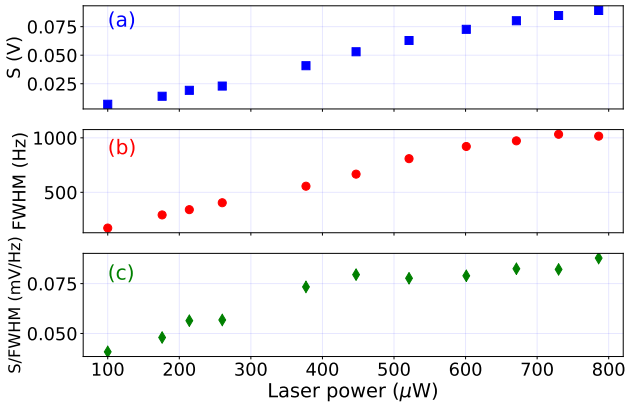

Fig. 5. (Color online) Signal (a), FWHM (b) and S/FWHM (c) of the dispersive CPT signal versus the laser power. The cell temperature is 28°C.

S/FWHM ratio for power values higher than 400 μW.

C. Residual phase noise

Following these basic spectroscopy tests, we have investigated the application of this detection scheme for demonstration of atomic clock operation. In this detection scheme, the residual phase noise of the microwave setup limits the ultimate achievable fractional frequency stability $\sigma_y(1s)$ of the clock. A residual phase fluctuation $\delta\varphi$ of the setup is converted through the mixer sensitivity k_D into a voltage fluctuation. The latter is then converted into a frequency fluctuation through the dispersive signal slope $S_l = S/\Delta\nu$. The ultimate clock fractional frequency stability at 1 s is then:

$$\sigma_y(1s) \simeq \frac{1}{\nu_0}\frac{\delta\varphi k_D}{S_l} \quad (5)$$

with ν_0 being the clock frequency.
We measured the residual phase noise at 9.192 GHz of key components of the microwave setup. For this purpose, a FFT analyzer is placed at the output of the dc amplifier that follows the microwave mixer. For all measurements, the microwave power at the inputs of the mixer, used as a phase detector, is in the 5 - 10 dBm range [36]. Since many components can induce a phase

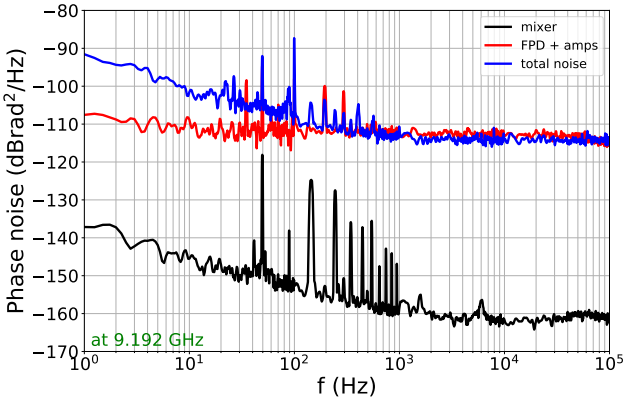

Fig. 6. (Color online) Residual phase noise of key components of the setup. mixer: microwave mixer, FPD + amps : photodetection stage including the fast photodiode and three microwave amplifiers in serial configuration. total noise: total residual phase noise. For the latter measurement, the whole setup shown in Fig. 1 is mounted. Blue curves and red curves were measured for similar microwave power at the output of the fast photodiode.

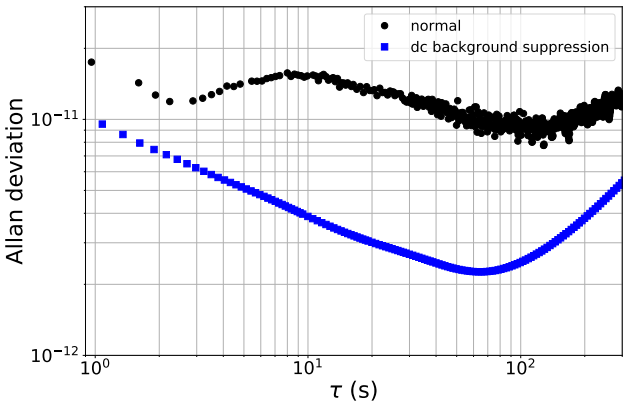

Fig. 7. (Color online) Allan deviation (all tau) of the CPT clock with the microwave phase detection technique, in normal operation (black circles) or with active dc background suppression (blue squares).

shift due to air movement, all measurements were performed by enclosing the whole table-top experiment within a thermal foam box. Without this precaution, phase noise spectra reported below could be strongly degraded, especially for offset frequencies lower than 30 - 40 Hz. Phase noise results are reported on Fig. 6. The residual phase noise of the microwave mixer is about -135 dBrad^2/Hz at $f = 1$ Hz. The red curve shows the phase noise of the total photodetection stage including the fast photodiode followed by three microwave amplifiers, in serial configuration. The phase noise spectrum of this stage is almost flat from 1 to 100 kHz. This trend is due to the high noise floor level, explained by the low microwave power (about -57 dBm for this test) at the input of the amplification stage [37] that follows the fast photodiode. At 1 Hz offset frequency, the phase noise level is about -108 dBrad^2/Hz. From additional measurements (not reported here), we found that this value is limited by the amplification stage and not by the photodiode [38]. We measured then the residual phase noise of the complete setup, with or without the CPT cell. In both cases, as shown in the example of Fig. 6 (blue curve), the residual phase noise is about $-$ 90 dBrad^2/Hz at $f = 1$ Hz. We suspect that the flicker part of the residual phase noise of our setup is limited by the conjunction of the frequency divider by 2, the high-power microwave amplifier and the EOM.

D. Short-term stability tests

We have used the dispersive CPT signal to directly stabilize the frequency of a microwave synthesizer, used as local oscillator, onto the atomic frequency. For this purpose, the error signal at the output of the mixer is acquired by a data acquisition card (DAQ) and processed digitally to send the corrections to the local oscillator frequency.

Figure 7 shows the Allan deviation of the CPT clock, in two different conditions, using the microwave phase detection technique, for a laser power at the cell input of 250 μW. In the first case (black circles, normal operation), the clock Allan deviation follows a plateau at a level between 1 - 2 $\times$ 10^{-11}, in good agreement with a flicker frequency-floor limited stability (with $k_D = 0.215$ V/rad, $\delta\varphi = 10^{(-90/20)} = 3.2 \times 10^{-5}$ rad and $S_l = 5.6 \times 10^{-5}$ V/Hz, $\sigma_y(1s) \simeq 1.3 \times 10^{-11}$ in Eq. (5)). This behaviour is compatible with the $1/f$ phase noise measured in Fig. 6 for $f < 100$ Hz (blue curve), indicating a flicker frequency noise of the microwave signal at the cell input [39].

We have then implemented an active suppression of the dc background level on which the symmetrical dispersive CPT signal was detected, in order to correct for the excess phase noise introduced by the experimental setup. For this purpose, the dc background signal was routinely measured off the CPT resonance (frequency jumps of $\pm$ 8 kHz) and subtracted from the mixer output. In these conditions, we have obtained an Allan deviation reaching about 1×10^{-11} at 1 s and averaging down to about 2×10^{-12} at 60 s (see blue curve on Fig. 7).

For integration times higher than 60 s, the Allan deviation is degraded. This degradation was probably due to temperature variations of the complete setup but also to the fact that the EOM bias point and laser power were not actively stabilized.

Short-term stability results reported here are about two orders of magnitude worse than those of state-of-the-art CPT based atomic clocks [10, 11, 13], using a standard optical transmission detection scheme, and comparable to those predicted from phase noise performances of a self-sustained cell-based microwave feedback oscillator [27]. With the present microwave phase detection scheme, the main challenge will be to reduce the setup residual phase noise. Achieving a total residual flicker phase noise of -120 dBrad^2/Hz at 1 Hz (for a carrier of about 10 GHz) is probably a reasonable objective, with the use of finely-selected low phase noise amplifiers [37], photodiodes [38, 40, 41] and electro-optic modulator [42]. In this case, keeping the same clock signal parameters, the clock stability at 1 s should reach the level of 4.1 $\times$ 10^{-13}, that is close to performances demonstrated by the best currently-available CPT clocks [10, 11, 13]. Finally, an interesting approach to explore, inspired from those described in [43–45], might be to split the light at the EOM output and optically mix two laser beams, one obtained at the cell output and another one that did not experience the atoms' phase shift.

5. CONCLUSIONS

We have reported on a microwave phase-sensitive detection scheme for spectroscopy of coherent-population trapping resonance in a Cs vapor cell. The approach consists of mixing the

optically-carried microwave signal that crossed the vapor cell and experienced the atom-induced phase shift with the probing interrogation signal itself such that a dispersive CPT error signal can be directly obtained. A qualitative model was developed to predict the phase shift between both laser fields at the cell output. The impact of the laser power onto the dispersive CPT signal was briefly studied. The dispersive error signal was used to stabilize the frequency of a local oscillator onto the CPT resonance. A short-term fractional frequency stability of 10^{-11} at 1 s was demonstrated, limited by the residual phase noise of the setup (EOM stage).

FUNDING

This work has been partly funded by Région Bourgogne Franche-Comté with the HACES project (grant 2018-04768), by the Délégation Générale de l'Armement (DGA), Agence Innovation Défense (AID), and in part by Agence Nationale de la Recherche (ANR) in the frame of the LabeX FIRST-TF (Grant ANR 10-LABX-0048), EquipX Oscillator-IMP (Grant ANR 11-EQPX-0033), ASTRID PULSACION (Grant ANR-19-ASTR-0013-01) and EIPHI Graduate school (Grant ANR-17-EURE-0002) projects.

ACKNOWLEDGMENTS

The authors would like to thank Clément Lacroute, Marion Delehaye, Vincent Giordano, Jacques Millo, Damien Teyssieux and Enrico Rubiola, at FEMTO-ST, for instructive discussions, and Christophe Fluhr (FEMTO-ST) for lending a frequency divider by 2. The authors also acknowledge Claudio Calosso and Salvatore Micalizio (INRIM) for fruitful discussions.

DISCLOSURES

The authors declare no conflicts of interest.

DATA AVAILABILITY STATEMENT

The data that support the findings of this study are available from the corresponding author upon reasonable request.

REFERENCES

1. G. Alzetta, A. Gozzini, L. Moi and G. Orriols, An experimental method for the observation of r.f. transitions and laser beat resonances in oriented Na vapour, Nuovo Cimento B **36**, 5-20 (1976).
2. R. M. Whitley and C. R. Stroud Jr., Double optical resonance, Phys. Rev. A **14,** 1498-1513 (1976).
3. E. Arimondo, Coherent population trapping in laser spectroscopy, Prog. Opt., **35,** 259-354 (1996).
4. B. J. Dalton and P. L. Knight, J. Phys. B **15,** 3997 (1982).
5. R. Wynands and A. Nagel, Precision spectroscopy with coherent dark states, Appl. Phys. B, **20**, 1-25 (1999).
6. J. Vanier, Atomic clocks based on coherent population trapping: a review, Appl. Phys. B Lasers Opt. **81,** DOI: 10.1007/s00340-005-1905-3 (2005).
7. S. Knappe, R. Wynands, J. Kitching, H. G. Robinson and L. Hollberg, Characterization of coherent population-trapping resonances as atomic frequency references, J. Opt. Soc. Am. B **18,** 11, 1545-1553 (2001).
8. A. Godone, F. Levi, S. Micalizio and C. Calosso, Coherent-population-trapping maser: Noise spectrum and frequency stability, Phys. Rev. A **70,** 012508 (2004).
9. M. Abdel Hafiz, G. Coget, P. Yun, S. Guérandel, E. De Clercq and R. Boudot, A high-performance Raman-Ramsey Cs vapor cell atomic clock, J. Appl. Phys. **121**, 104903 (2017).
10. P. Yun, F. Tricot, C. E. Calosso, S. Micalizio, B. Francois, R. Boudot, S. Guérandel and E. de Clercq, High-Performance Coherent Population Trapping Clock with Polarization Modulation, Phys. Rev. Applied **7,** 014018 (2017).
11. M. Abdel Hafiz, G. Coget, M. Petersen, C. E. Calosso, S. Guérandel, E. De Clercq and R. Boudot, Symmetric autobalanced Ramsey interrogation for high-performance coherent population- trapping vapor-cell atomic clock, Appl. Phys. Lett. **112**, 244102 (2018).
12. X. Liu, E. Ivanov, V. I. Yudin, J. Kitching and E. A. Donley, Low-drift coherent population trapping Clock based on laser-cooled atoms and high-coherence excitation fields, Phys. Rev. Appl. **8**, 054001 (2017).
13. P. Yun, Q. Li, Q. Hao, G. Liu, E. de Clercq, S. Guérandel, X. Liu, S. Gu, Y. Gao and S. Zhang, High-performance coherent population trapping atomic clock with direct-modulation distributed Bragg reflector laser, Metrologia **58**, 045001 (2021).
14. P. D. D. Schwindt, S. Knappe, V. Shah, L. Hollberg and J. Kitching, Chip-scale atomic magnetometer, Appl. Phys. Lett. **85**, 26, 6409-6411 (2004).
15. E. Breschi, Z. D. Gruji, P. Knowles and A. Weis, A high-sensitivity push-pull magnetometer, Appl. Phys. Lett. **104**, 023501 (2014).
16. M. Bajcsy, A. S. Zibrov and M. D. Lukin, Stationary pulses of light in an atomic medium, Nature **426,** 638-641 (2003).
17. A. Aspect, E. Arimondo, R. Kaizer, N. Vansteenkiste and C. Cohen-Tannoudji, Laser cooling below the one-photon recoil energy by velocity-selective coherent population trapping: theoretical analysis, J. Opt. Soc. Am. B **6**, 2112-2124 (1989).
18. G. J. Dick, J. D. Prestage, C. A. Greenhall, and L. Maleki, Local oscillator induced degradation of medium-term stability in passive atomic frequency standards, in Proc. 22nd Precise Time and Time Interval (PTTI) Applications and Planning Meeting, 1990, pp. 487–508.
19. G. Santarelli, C. Audoin, A. Makdissi, P. Laurent, G. J. Dick, and A. Clairon, Frequency stability degradation of an oscillator slaved to a periodically interrogated atomic resonator, IEEE Trans. Ultrason. Ferroelectr. Freq. Control **45**, 4, 887-894 (1998).
20. J. M. Danet, M. Lours, S. Guérandel and E. de Clercq, Dick effect in a pulsed atomic clock using coherent population trapping, IEEE Trans. Ultrason. Ferroelectr. Freq. Control **61**, 4, 567-574 (2014).
21. C. Audoin, V. Candelier, N. Dimarcq, A limit to the frequency stability of passive frequency standards due to an intermodulation effect, IEEE Trans. Intr. Meas. **40**, 2, 121-125 (1991).
22. V. I. Yudin, A. Taichenachev, D. Sevostianov, V. Velichansky, V. Vassiliev, A. Zibrov, A. Zibrov, S. Zibrov, Feedback spectroscopy of atomic resonances, Phys. Rev. A **87**, 063608 (2013).
23. N. Vukicevic, A. S. Zibrov, L. Hollberg, F. L. Walls, J. Kitching and H. G. Robinson, Compact diode-laser based rubidium frequency reference, IEEE Trans. Ultrason. Ferroelec. Freq. Contr. **47,** 5, 1122-1126 (2000).
24. D. Strekalov, D. Aveline, N. Yu, R. Thompson, A.B. Matsko and L. Maleki, Stabilizing an optoelectronic microwave oscillator with photonic filters, IEEE Jour. Light. Tech **21,** 12, 3052-3061 (2003).
25. A.B. Matsko, D. Strekalov and L. Maleki, Magnetometer based on the optoelectronic oscillator, Opt. Comm. **247,** 141 (2005).
26. D. Strekalov, A. B. Matsko, N. Yu, A. A. Savchenkov and L. Maleki, Application of vertical cavity surface emitting lasers in self-oscillating atomic clocks, J. Mod. Opt. **53,** 16-17, 2469-2484 (2006).
27. R. Boudot, M. Abdel Hafiz, M. Petersen, C. Calosso and E. Rubiola, All-optical microwave feedback oscillator with atomic cell resonator, Appl. Phys. Lett. **120,** 044101 (2022).
28. M. Abdel Hafiz, G. Coget, E. de Clercq and R. Boudot, Doppler-free spectroscopy on the Cs D_1 line with a dual-frequency laser, Opt. Lett. **41,** 2982 (2016).
29. D. Brazhnikov, M. Petersen, G. Coget, N. Passilly, V. Maurice, C.

Gorecki and R. Boudot, Dual-frequency sub-Doppler spectroscopy: Extended theoretical model and microcell-based experiments, Phys. Rev. A **99,** 062508 (2019).
30. Y. Y. Jau, E. Miron, A. B. Post, N. N. Kuzma and W. Happer, Push-Pull Optical Pumping of Pure Superposition States, Phys. Rev. Lett. **93,** 160802 (2004).
31. J. Vanier, A. Godone, and F. Levi, Coherent population trapping in cesium: Dark lines and coherent microwave emission, Phys. Rev. A **58** , 2, 2345-2357 (1998).
32. J. Vanier and C. Audoin, "The quantum physics of atomic frequency standards", Adam Hilger, Bristol (1989)
33. J. B. Taylor, and I. Langmuir, Vapor pressure of caesium by the positive ion method, Phys. Rev. **51** , 9, 753-760 (1937).
34. G. A. Pitz, D. E. Wertepny, and G. P. Perram, Pressure broadening and shift of the Cs D_1 transition by the noble gases and: N_2, H_2, HD, D_2, CH_4, C_2H_6, CF_4, and ^{3}He, Phys. Rev. A, 80:062718 (2009).
35. O. Kozlova, S. Guérandel and E. de Clercq, Temperature and pressure shift of the Cs clock transition in the presence of buffer gases: Ne, N_2, Ar, Phys. Rev. A **83,** 062714 (2011).
36. E. Rubiola, Tutorial on the double-balanced mixer, arXiv:physics/0608211v1 (2006).
37. R. Boudot and E. Rubiola, Phase noise in RF and microwave amplifiers, IEEE Trans. Ultrason. Ferroelec. Freq. Contr. **59**(12), 2613-2624 (2012).
38. E. Rubiola, E. Salik, N. Yu and L. Maleki Flicker noise in high-speed photodetectors, IEEE Trans. Microwave Theory Tech. **54**(2), 816-820 (2006).
39. E. Rubiola, Phase noise and frequency stability in oscillators, The Cambridge RF and microwave engineering series (2010).
40. T. M. Fortier, F. Quinlan, A. Hati, C. Nelson, J. A. Taylor, Y. Fu, J. Campbell, and S. A. Diddams, Photonic microwave generation with high-power photodiodes, Opt. Lett. **38** , 10, 1712-1714 (2013).
41. D. Lee, T. Nakamura, J. Zang, J. C. Campbell, S. A. Diddams and F. Quinlan, Reduction of flicker phase noise in high-speed photodetectors under ultrashort pulse illumination, IEEE Photonics Journal **13** , 3 (2021).
42. K. Volyansky, J. Cussey; H. Tavernier, P. Salzentein, G. Sauvage, L. Larger and E. Rubiola, Applications of the optical fiber to the generation and measurement of low-phase-noise microwave signals, J. Opt. Soc. Am. B **25**(12), 2140-2150 (2008).
43. J. Lodewyck, P. Westergaard and P. Lemonde, Nondestructive measurement of the transition probability in a Sr optical lattice clock, Phys. Rev. A **79**, 061401(R) (2009).
44. T. Vanderbruggen, R. Kohlhaas, A. Bertoldi, S. Bernon, A. Aspect, A. Landragin and P. Bouyer, Feedback Control of Trapped Coherent Atomic Ensembles, Phys. Rev. Lett. **110**, 210503 (2013).
45. R. Kohlhaas, A. Bertoldi, E. Cantin, A. Aspect, A. Landragin and P. Bouyer, Phase Locking a Clock Oscillator to a Coherent Atomic Ensemble, Phys. Rev. X **5**, 021011 (2015).